NUCL SCI TECH (2022) 33:58
https://doi.org/10.1007/s41365-022-01050-w

# Isospin effects on intermediate mass fragments at intermediate energy-heavy ion collisions

**Li Li[1] · Fang-Yuan Wang[1] · Ying-Xun Zhang[1,2]**

Received: 29 March 2022 / Revised: 23 April 2022 / Accepted: 25 April 2022 / Published online: 15 June 2022


**Abstract** In this study, we investigated the isospin properties of intermediate mass fragments (IMFs) for the central collisions of $^{112,124}$Sn+$^{112,124}$Sn at a beam energy of 50 MeV per nucleon using an improved quantum molecular dynamics model (ImQMD) coupled with a sequential decay model (GEMINI). Three observables were analyzed: (1) the average center-of-mass kinetic energy per nucleon $\langle E_{\mathrm{c.m.}}/A\rangle$ of fragments as a function of their charge number $Z$; (2) the average neutron number to proton number ratio ($\langle N\rangle/Z$) of fragments with a given charge number $Z$ as a function of their center-of-mass kinetic energy per nucleon ($E_{\mathrm{c.m.}}/A$); and (3) the average total neutron number to total proton number ratio ($\sum N/\sum Z$) and double ratio ($DR(N/Z)$) of IMFs with $Z$ = 3–8 as a function of their center-of-mass kinetic energy per nucleon $E_{\mathrm{c.m.}}/A$. Our calculations revealed that the sensitivity of the isospin properties of IMFs relative to the stiffness of the symmetry energy remains even after sequential decay. By comparing the calculations of $\sum N/\sum Z$ and $DR(N/Z)$ with the data, it was found that the soft symmetry energy, i.e., $\gamma = 0.5$, is favored.

**Keywords** Symmetry energy · Intermediate mass fragments · Isospin effects

## 1 Introduction

The Equation of State (EOS) of asymmetric nuclear matter can be written approximately as

$$E(\rho,\delta) = E_0(\rho,\delta=0) + S(\rho)\delta^2 + O\left(\delta^4\right) + \cdots, \quad (1)$$

where $\delta = \left(\rho_{\mathrm{n}} - \rho_{\mathrm{p}}\right)/\left(\rho_{\mathrm{n}} + \rho_{\mathrm{p}}\right)$, which is related to different areas of nuclear physics, such as the nuclear structure of ground-state nuclei, the dynamics of neutron-rich heavy ion collisions (HICs), the physics of neutron stars, etc. [1, 2]. To date, the isoscalar component of the EOS has been well-constrained by the kaon condensation and the flow data of HICs [3]. However, the symmetry energy, particularly the density dependence of the symmetry energy $S(\rho)$, still has large uncertainties away from the normal density.

Heavy-ion collisions with neutron-rich nuclei in facilities, such as the Heavy Ion Research Facility in Lanzhou (HIRFL/Lanzhou), Facility for Rare Isotope Beams at Michigan States University (FRIB/MSU), the Radioactive Isotope Beam Factory (RIBF/RIKEN), will produce rare isotope beams to study the dynamical evolution of neutron-rich nuclear systems and obtain information on the density dependence of the symmetry energy by comparing the acquired data with the transport model simulations [4, 5]. Many theoretical and experimental studies have been conducted to constrain the density dependence of the

This work was supported by the National Natural Science Foundation of China (Nos. 11875323, 11705163, 11790320, 11790323, and 11961141003), the National Key R&D Program of China (No. 2018 YFA0404404), the Continuous Basic Scientific Research Project (Nos. WDJC-2019-13, BJ20002501), funding from the China Institute of Atomic Energy and the Leading Innovation Project of CNNC (Nos. LC192209000701 and LC202309000201).

✉ Ying-Xun Zhang
zhyx@ciae.ac.cn

[1] China Institute of Atomic Energy, P. O. Box 275(18), Beijing 102413, China

[2] Department of Physics and Technology, Guangxi Normal University, Guilin 540101, China

symmetry energy via intermediate-energy HICs [2, 6–20]. In addition, Zheng et al. proposed a novel method for studying the symmetry energy [21], which may impose additional restriction on the constraints in the future. There are also a lot of studies that aim to constrain the density dependence of symmetry energy at the suprasaturation density by analyzing the properties of neutron stars, such as the mass-radius relationship and tidal deformability [23–34], subsequent to the publication of GW170817 events data [23, 24]. By analyzing the combination of the observables of the neutron skin of $^{208}$Pb, the collective flow, isospin diffusion, or $\pi^-/\pi^+$ ratios of HICs, and properties of neutron stars, the relatively tight constraints on the symmetry energy were inferred from $0.3\rho_0$ to $3\rho_0$ [12, 14, 17, 22]. In a recent review paper by Li et al. [35], the constraints on the symmetry energy were compiled and yielded the average values and their variances. For the slope of the symmetry energy, i.e., $L = 3\rho_0 \frac{\partial S(\rho)}{\partial \rho}\big|_{\rho_0}$, the value is $57.7 \pm 19$ MeV, and the symmetry energy at twice the normal density $S(2\rho_0)$ is $51 \pm 13$ MeV.

However, there is tension around the symmetry energy constraints following the Lead Radius Experiment (PREX-II) reporting of a model-independent extraction of the neutron skin of $^{208}$Pb and $\Delta r_{\rm np} = 0.283 \pm 0.071$ fm [36]. Yue et al. [17] analyzed newly published neutron skin data with ground-state properties and giant monopole resonances of finite nuclei, the properties of neutron stars for PSR J0740+6620, the mass-radius of PSR J0030+045, and the neutron star tidal deformability extracted from the GW170817 event to obtain the constraints of symmetry energy in a large density region. Their calculations suggested that $S(\rho_0) = 34.5 \pm 1.5$ MeV and $L = 85.5 \pm 22.2$ MeV. The values obtained are consistent with the constraints of the symmetry energy from the SπRIT data [13] for Sn+Sn at 270A MeV, but are less than the values obtained for the analysis of PREX-II using a specific class of relativistic energy density functional [36], in which $L = 106 \pm 37$ MeV and $S_0 = 38.7 \pm 4.7$ MeV. Their constraints on the symmetry energy also overlap with the symmetry energy extracted from the charge radius of $^{54}$Ni, where 21 MeV $< L <$ 88 MeV [37], and the combination of astrophysical data with PREX-II and chiral effective field theory, where $L = 53^{+14}_{-15}$ MeV [38].

Currently, the big challenge in constraining the density dependence of the symmetry energy with HICs is to understand the model dependence and reduce the uncertainties of the symmetry energy constraints. The understanding of the model dependence has been achieved in the last 10 years via the transport model evaluation project, and significant progress has been made in the treatment of nucleon-nucleon collisions and the mean-field potential [39–43]. The reduction in the uncertainties of symmetry energy constraints is still underway, which can be realized by simultaneously describing multi-observables using transport models. The data for isospin-sensitive observables from intermediate-energy HICs, such as isoscaling [44], double neutron to proton ratio [45], isospin diffusion [46], rapidity dependence of the isobaric ratio [10], and neutron-excess to proton ratio [11], have been used for comparison with the predictions from different transport models [4, 5]. Among these transport models, the ImQMD model successfully describes the neutron-to-proton yield ratio (n/p ratio), isospin diffusion, and isospin transport ratio as a function of rapidity, and constraints on the symmetry energy at the subsaturation density have been achieved [5].

Except for the aforementioned isospin-sensitive observables, the neutron number divided by the proton number of IMFs was considered to be complementary information of the neutron-to-proton yield ratio and can be used to extract information related to the symmetry energy [6]. This can be explained by the multi-fragmentation mechanism where the copious production of IMFs and its isospin contents are closely related to the dynamic mechanism of the HICs [47–49].

The measurement of IMFs has been performed at the National Superconducting Conducting Cyclotron Laboratory at Michigan State University [50], but there are few models for the theoretical analysis of the isospin effects of IMFs and their use to constrain the symmetry energy. Thus, it is worth to check whether the ImQMD model can simultaneously describe the isospin properties of IMFs.

In this study, we focus on the properties of IMFs ($Z = 3 - 8$) for the central collision ($b = 2$ fm) of $^{112,124}$Sn + $^{112,124}$Sn at $E_{\rm beam}$=50 MeV/u using the ImQMD model coupled with the GEMINI model. Furthermore, we compared the calculated results to the data for learning the form of the symmetry energy and the reaction dynamics.

## 2 Theoretical model and symmetry energy

The version of ImQMD used in this study was the same as that used in Ref. [5], i.e., ImQMD05, in which the isospin-independent momentum-dependent interaction was utilized. To simulate low-intermediate energy HICs, the basic properties of the initial nuclei are important, and they are guaranteed by requiring that the binding energy and root-mean-square (rms) radius of the sampled nuclei fall within the range of the experimental data with specific uncertainties. For the standard initialization treatment, the initial nuclei remain stable within 200 fm/$c$, which is sufficient for Sn+Sn at 50 MeV/u because the reaction

dynamics are completed within 100 fm/$c$ [51]. Additional details regarding the initialization of the ImQMD model can be found in Refs. [51–55].

The nucleonic mean field potential is derived from the Skyrme-type energy density functional, and the energy density of the symmetry potential is as follows:

$$w_{\mathrm{asy}}^{\mathrm{pot}} = \frac{C_{\mathrm{S}}}{2}\left(\frac{\rho}{\rho_0}\right)^{\gamma}\delta^2\rho. \tag{2}$$

where $\rho$ is the nucleon density. $C_{\mathrm{S}}$ is the symmetry potential parameter, $C_{\mathrm{S}} = 35.2$ MeV, and $\gamma$ is a parameter related to the density dependence of the symmetry energy. Based on these interaction parameters, we can obtain the symmetry energy per nucleon for cold nuclear matter, as follows:

$$S(\rho) = \frac{1}{3}\frac{\hbar^2}{2m}\rho_0^{2/3}\left(\frac{3\pi^2}{2}\frac{\rho}{\rho_0}\right)^{2/3} + \frac{C_{\mathrm{S}}}{2}\left(\frac{\rho}{\rho_0}\right)^{\gamma}, \tag{3}$$

where $m$ denotes the nucleon mass. The corresponding values of the symmetry energy $S(\rho_0)$ and the slope of the symmetry energy $L = 3\rho_0\frac{\partial S(\rho)}{\partial\rho}\big|_{\rho_0}$ at a normal density are listed in Table 1. For this particular parameterization, the symmetry energy increases with a decrease of $\gamma$ at a sub-saturation density, whereas the opposite is true for supra-normal density.

The ImQMD simulations were terminated at 400 fm/$c$ when the systems reached "dynamical freeze-out." The primary fragments were recognized using the isospin-dependent minimum spanning tree method [51], and the excitation energy was calculated in the rest frame of the fragment by subtracting the ground state energy from the energy of the fragment in its rest frame. It should be noted that the fragments produced during the ImQMD calculations are primary, and they may have very neutron-rich or very neutron-poor "unphysical" fragments. The probability of generation of these "unphysical" primary fragments is tiny in ImQMD simulations, and their ground state energies are approximately obtained using the liquid-drop mass formula.

The sequential decay of the primary fragments was performed using the GEMINI code [56, 57], which describes the de-excitation process of the compound nucleus and facilitates binary decay, including light-particle evaporation and symmetric fission. The decay continues until the particle emission is energetically forbidden or impossible owing to competition with $\gamma$-ray emission.

**Table 1** The symmetry energy coefficient and slope of the symmetry energy correspond to the parameters used in ImQMD05. $S_0$, $L$ and $S(2\rho_0)$ are in MeV, $\gamma$ is dimensionless

| *Para* | $S_0$ | $L$ | $S(2\rho_0)$ |
|---|---|---|---|
| $\gamma = 0.5$ | 30 | 51 | 44.4 |
| $\gamma = 2.0$ | 30 | 130 | 90.0 |

## 3 Results and discussions

Before studying the isospin properties of the IMFs, we focused on the cluster formation mechanism of HICs. Figure 1 shows the time evolution of the multiplicities of emitted nucleons (top panels) and fragments (bottom panels), for the collisions of $^{124}$Sn $+^{124}$ Sn and $^{112}$Sn $+^{112}$ Sn. It is evident that the nucleons are emitted prior to IMFs with $Z = 3-8$, and IMFs with $Z = 3-8$ prior to fragments with $Z = 9-20$. For example, for the reaction system $^{112}$Sn+$^{112}$Sn, the emission of nucleons begins from $t \sim 50$ fm/$c$, but the emission of IMFs with $Z = 3-8$ occurs at approximately $t \sim 100$ fm/$c$ and $Z = 9-20$ fragments at approximately $t \sim 140$ fm/$c$. Such a dynamic process results in a decrease in the fragment velocity with the fragment charge number. After $t \sim 250$ fm/$c$, the primary fragments are completely formed. Ideally, the system should be in "dynamical freeze-out," and its multiplicities should not change with time. However, it is difficult for the QMD type Hamiltonian to bind the fragments for a long time, and the pseudo-emission of nucleons occurs at the late stage of the simulations of HICs. Therefore, the multiplicities of fragments with $Z = 3-8$ or $9-20$ decrease slightly, and the magnitude depends on the stiffness of the symmetry energy.

To understand the influence of different symmetry potentials on the reaction dynamics, we investigated the time evolution of the multiplicities of nucleons and fragments for $\gamma = 0.5$ (solid lines) and $\gamma = 2.0$(dashed lines). The results show that the multiplicities of the nucleons and the fragments depend on $\gamma$ and the isospin asymmetry of the reaction system.

The multiplicities of emitted neutrons calculated with $\gamma = 0.5$ are greater than those with $\gamma = 2.0$, and the effect is the opposite for the multiplicities of protons. Consequently, it is expected that the neutron-to-proton yield ratio would be sensitive to the stiffness of the symmetry energy. Numerous studies have investigated for constraining the symmetry energy using $n/p$ ratios [10, 39, 45, 54, 58, 59].

For the multiplicities of fragments with $Z = 3-8$ (or 9-20), the calculations show that the multiplicities of IMFs obtained with $\gamma = 0.5$ are smaller than those with $\gamma = 2.0$. This is because a higher density is reached in the overlap region and more compressional energy is stored for the soft isospin asymmetric nuclear equation of the state ($\gamma = 0.5$) compared to that of the stiff isospin asymmetric nuclear

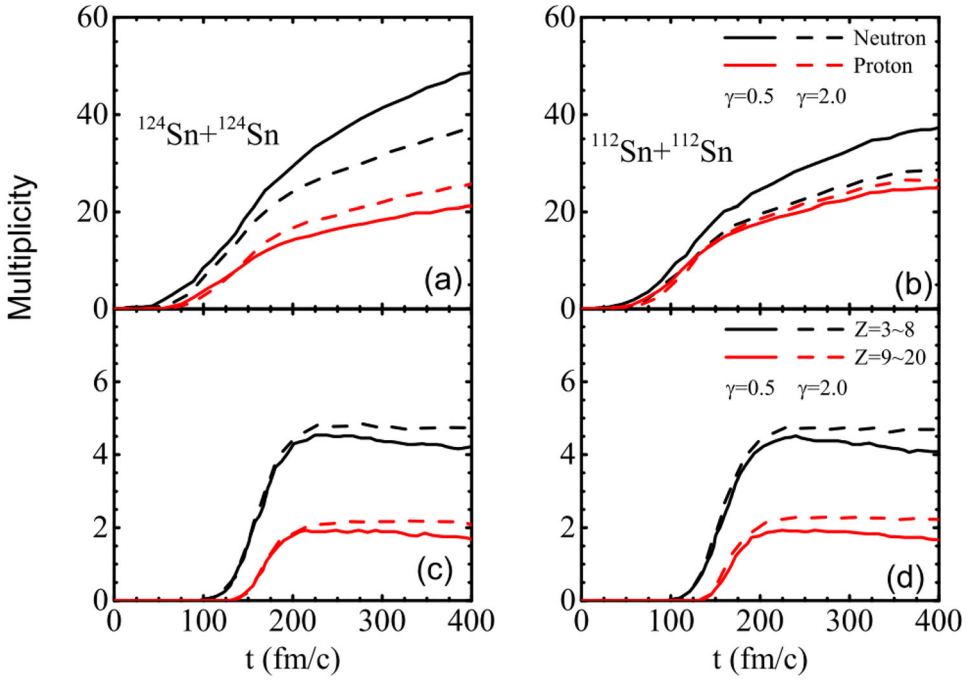


**Fig. 1** (Color online) The time evolution of the multiplicities of nucleons and fragments with $Z = 3 - 8$ and $Z = 9 - 20$ for $^{124}$Sn $+^{124}$ Sn (panels **a** and **c**) and $^{112}$Sn $+^{112}$ Sn (panels **b** and **d**) for different symmetry energy cases

equation of state ($\gamma = 2.0$) in the simulations. Thus, the reaction system simulated with $\gamma = 0.5$ disintegrates into more light-charged fragments compared to the case of $\gamma = 2.0$. Owing to the conservation of the nucleon number in the reaction system, the multiplicities for fragments with $Z = 3 - 8$ (or 9-20) for the $\gamma = 0.5$ case are smaller than those for $\gamma = 2.0$.

Considering the reaction dynamics, it is expected that the size of the fragments and their kinetic energies should be correlated to the stiffness of the symmetry energy. In Fig. 2, the average center-of-mass kinetic energy per nucleon $\langle E_{\mathrm{c.m.}}/A \rangle$ is plotted for the primary fragments as a function of their charge number $Z$ for $^{124}$Sn+$^{124}$Sn (left panel),and $^{112}$Sn+$^{112}$Sn (right panel). The solid red lines represent the calculated results for $\gamma = 0.5$, and the dashed red lines are the results obtained for $\gamma = 2.0$. For both symmetry energies, the values of $\langle E_{\mathrm{c.m.}}/A \rangle$ decrease with an increase in $Z$ owing to the aforementioned reaction dynamics. It is interesting to note that $\langle E_{\mathrm{c.m.}}/A \rangle$ as a function of $Z$ is also sensitive to the density dependence of the symmetry energy, and the values of $\langle E_{\mathrm{c.m.}}/A \rangle$ obtained for $\gamma$=0.5 are larger than those obtained for $\gamma = 2.0$ when $Z > 3$. This can be understood based on the reaction dynamics shown in Fig. 1, wherein the multiplicities of the IMFs are larger for $\gamma = 2.0$ compared to the case of $\gamma = 0.5$. If there is an energy equipartition about

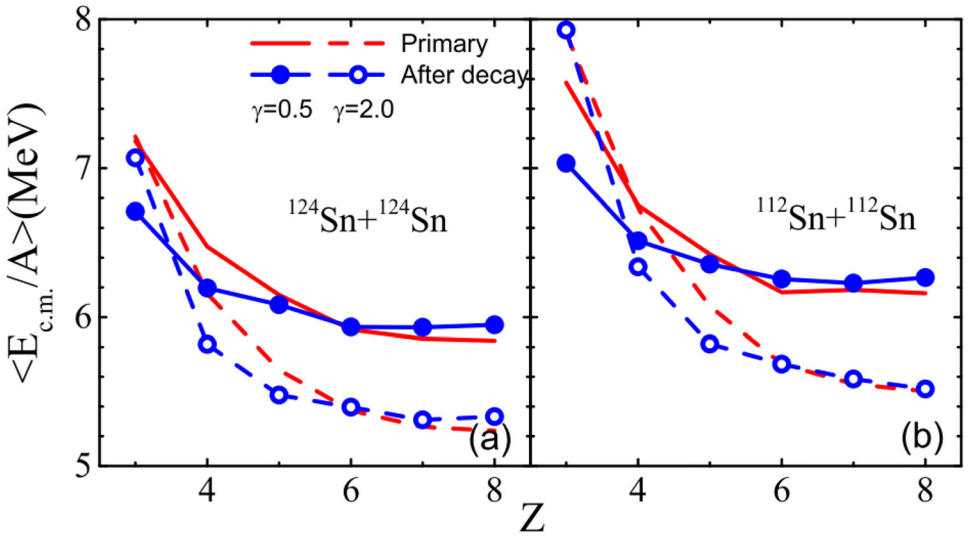


**Fig. 2** (Color online) The average kinetic energy per nucleon as a function of the fragment charge number $Z$. The solid symbols represent $\gamma = 0.5$ and the open circles represent $\gamma = 2.0$. The red lines are the results for primary fragments, and the blue lines with symbols represent the cold fragments

fragments, one can expect each IMF to carry less kinetic energy for the case of $\gamma = 2.0$ compared to the case of $\gamma = 0.5$. The difference between the values of $\langle E_{\mathrm{c.m.}}/A \rangle$ obtained for $\gamma = 0.5$ and $\gamma = 2.0$ increase with an increase in $Z$, and the difference exceeds 10% at $Z = 8$.

However, the measured fragments in the experiments were cold, which indicate that the hot primary fragments should be deexcited. In this study, the decay of the primary fragments created in the ImQMD simulations was performed using the GEMINI code [56, 57] using their default parameter sets. The blue lines with symbols represent the results for the cold fragments. For $Z = 3$ and 4, the values of $\langle E_{\mathrm{c.m.}}/A \rangle$ are reduced by $\sim$7% compared to the results obtained for the primary fragments. This reduction is caused by the decay of primary fragments, which converts the fragments with higher mass or charge numbers to those with lower mass or charge numbers. For fragments with $Z \geq 6$, the effects of decay on $\langle E_{\mathrm{c.m.}}/A \rangle$ are weak, and the sensitivities of $\langle E_{\mathrm{c.m.}}/A \rangle$ to the stiffness of the symmetry energy remain. Consequently, $\langle E_{\mathrm{c.m.}}/A \rangle$ as a function of $Z$ of the IMFs can also be used to understand the fragmentation mechanism and to probe the density dependence of the symmetry energy.

We will now discuss the isospin contents of the IMFs in more detail. The $\langle N \rangle/Z$ of the IMFs was investigated, which is defined as

$$\langle N \rangle/Z = \frac{\sum_i N_i \times Y(N_i, Z)}{\sum_i Y(N_i, Z)} \Big/ Z. \tag{4}$$

where $Y(N_i, Z)$ is the yield of the fragment with a neutron number $N_i$ and charge number $Z$. The summation is for all isotopes at a given $Z$. As an example, Fig. 3 presents the $\langle N \rangle/Z$ ratio of primary fragments (red lines) as a function of $E_{\mathrm{c.m.}}/A$ for fragments with $Z = 3, 4, 5, 6, 7, 8$. The left six panels are for $^{124}$Sn +$^{124}$ Sn and the right six panels are for the reaction system $^{112}$Sn +$^{112}$ Sn. In general, the slopes of the $\langle N \rangle/Z$ ratio as a function of $E_{\mathrm{c.m.}}/A$ are negative, because the Coulomb energy accelerates the neutron-poor fragments to a higher kinetic energy region. These behavior occurs for all elements of the IMFs. Furthermore, the curves of the $\langle N \rangle/Z$ ratios as a function of kinetic energy $E_{\mathrm{c.m.}}/A$ depend on the stiffness of the symmetry energy, and the results obtained for $\gamma = 0.5$ and 2.0 crossover at a specific energy, $E_{\mathrm{cross}}$. The values of $E_{\mathrm{cross}}$ increase from 4 MeV to approximately 10 MeV as $Z$ increases from 3 to 8, owing to the Coulomb interaction.

Below the cross-energy, the values of $\langle N \rangle/Z$ obtained for $\gamma = 0.5$ are smaller than those obtained for $\gamma = 2.0$, and turn over above $E_{\mathrm{cross}}$. The predicted magnitude of the slope of the $\langle N \rangle/Z$ ratio as a function of $E_{\mathrm{c.m.}}/A$ obtained for $\gamma$=0.5 is smaller compared to that for $\gamma = 2.0$. This behavior can be understood based on the cluster formation mechanism. For the $Z \leq 4$ fragments with high kinetic energy, and the isospin effects were governed by the dynamics. Thus, the behavior of $\langle N \rangle/Z$ of the fragments in the high kinetic energy region is similar to the *n/p* ratios of the emitted nucleons. Consequently, one can expect the values of $\langle N \rangle/Z$ obtained for $\gamma = 0.5$ to be larger than those obtained for $\gamma = 2.0$.

Fragments with low kinetic energy or heavier fragments are formed at a later stage of the reaction, and their isospin content is determined by their free energy. The free energy of the primary fragments, $f(A, \delta, T)$, can be approximated as

$$\begin{aligned} f(A, \delta, T) = & -a_{\mathrm{sym}}^{v}(\rho, T)(N - Z)^2/A + a_{\mathrm{sym}}^{\mathrm{surf}}(\rho, T)\delta^2 A^{2/3} \\ & - a_{\mathrm{c}}(\rho, T)Z(Z-1)/A^{1/3} \\ & + a_{\mathrm{v}}(\rho, T)A - a_{\mathrm{s}}(\rho, T)A^{2/3}. \end{aligned} \tag{5}$$

where $a_{\mathrm{sym}}^{\mathrm{v}}$ and $a_{\mathrm{sym}}^{\mathrm{surf}}$ are the bulk-and surface-related symmetry energy coefficients, respectively. $a_{\mathrm{c}}$ is a coefficient related to the Coulomb energy, and $a_{\mathrm{v}}$ and $a_{\mathrm{s}}$ are the volume and surface energy coefficients, respectively. If we assume that the fragments are at thermal equilibrium and stable, the isospin asymmetry of the primary fragment is determined by the minimum free energy of the cluster at temperature $T$, i.e., $\frac{\partial f(A,\delta,T)}{\partial \delta} = 0$. Therefore, the isospin asymmetry of the primary fragments should be proportional to

$$\delta_{\mathrm{frag}} = \frac{a_{\mathrm{c}}(\rho, T)A^{2/3}(A-1)}{a_{\mathrm{c}}(\rho, T)A^{5/3} + 4a_{\mathrm{sym}}^{\mathrm{v}}(\rho, T)A - 4a_{\mathrm{sym}}^{\mathrm{surf}}A^{2/3}}. \tag{6}$$

The Coulomb interaction increases the isospin asymmetry of the primary fragments and the symmetry energy term decreases the isospin asymmetry of the fragments. Since the fragments are formed during the expansion phase during which the system is at a subsaturation density, the values of the symmetry energy $a_{\mathrm{sym}}^{\mathrm{v}}(\rho, T)$ obtained for $\gamma$=0.5 are larger than those obtained for $\gamma$=2.0, and it is expected that the $\langle N \rangle/Z$ values of the fragments obtained for $\gamma$=2.0 will be larger than those for $\gamma$=0.5, according to Eq. (6).

To investigate the secondary sequential decay effects, we present $\langle N \rangle/Z$ as a function of $E_{\mathrm{c.m.}}/A$ as blue lines in Fig. 3. For fragments with $Z \geq 5$, the secondary decay reduces the sensitivity of $\langle N \rangle/Z$ to the stiffness of the symmetry energy because of abundant neutron evaporation. Specifically, the decay weakly influences the isospin contents of the fragments obtained for $\gamma$=0.5, and strongly

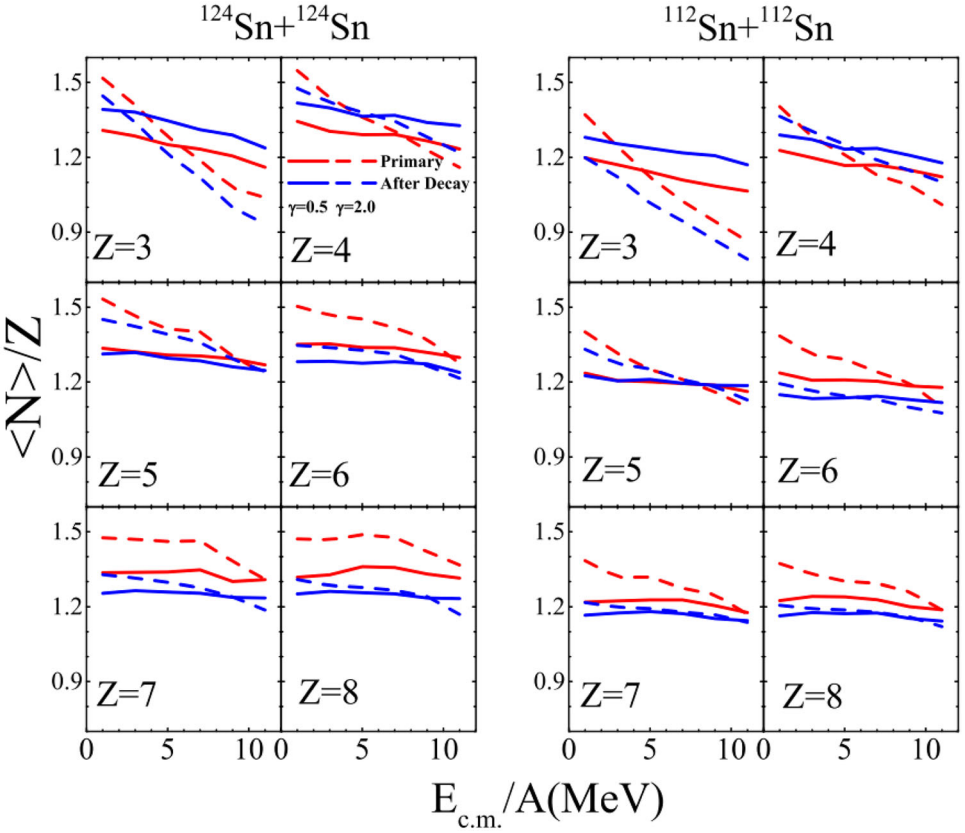


**Fig. 3** The $\langle N/Z \rangle$ ratios as functions of kinetic energy per nucleon for $Z$ = 3, 4, 5, 6, 7, 8 for primary (red lines) and cold fragments (blue lines) obtained for $\gamma = 0.5$ and 2.0. The left six panels are for $^{124}$Sn +$^{124}$ Sn, and the right panels are for $^{112}$Sn +$^{112}$ Sn

suppresses the $\langle N \rangle / Z$ obtained for $\gamma$=2.0. This is because the $E^*/A$ obtained for $\gamma = 0.5$ is smaller than that obtained for $\gamma = 2.0$. For $\gamma$=0.5, the values of $E^*/A$ varied from 1.6 to 1.8 MeV. For $\gamma$ =2.0, the values of $E^*/A$ varied from 1.8 to 2.4 MeV. The hardly understanding point is that the sensitivity of $\langle N \rangle / Z$ to the stiffness of the symmetry energy is the same or is enhanced for $Z = 3$ and 4 after the decay. This could be related to the "$^3$He $-^4$ He puzzle" [60–62] and the decay of $^8$Be [50]. Thus, the cluster formation mechanism in transport models and the sequential decay model require further refinement.

To avoid the cluster formation flaw in the transport model, we calculated $\sum N / \sum Z$ for fragments with $Z$ from 3 to 8. $\sum N$ and $\sum Z$ are defined as follows:

$$\sum N = \sum_{i,j} N_i \times Y(Z_j, N_i); \tag{7}$$

$$\sum Z = \sum_{i,j} Z_j \times Y(Z_j, N_i). \tag{8}$$

The summation is over all IMFs for a given kinetic energy bin (1.5 MeV/nucleon) for all events. This is similar to the method proposed in Ref. [6] for studying the isospin effects and symmetry energy in HICs.

The data on the isospin observable $\sum N / \sum Z$ for the central collision of Sn+Sn were reported in Ref. [50]. It should be noted that the experimental central collisions are defined by the high multiplicity of charged particles, and the corresponding real impact parameter distribution is Gaussian [63–65]. For the central collision events selected in Refs. [50], the reduced impact parameter ranges from 0 to approximately 0.4 and peaks at approximately 0.2. Thus, we performed simulations at a representative value of the impact parameter, such as the mean of the impact parameter distribution, $b = 2$ fm. We also selected fragments emitted at center-of-mass angles of $70° \leq \theta_{c.m.} \leq 110°$, which is the same as that in Ref. [50]. The calculated results are shown in Fig. 4a–d. Panels (a) and (c) show $^{124}$Sn +$^{124}$ Sn, and panels (b) and (d) show $^{112}$Sn +$^{112}$ Sn. The calculated results for $\sum N / \sum Z$ for the primary fragments (top panels) strongly depend on the density dependence of the symmetry, which is consistent with the results in Ref. [6]. However, $\sum N / \sum Z$ as a function of $E_{c.m.}/A$ obtained in the transverse direction is weakly sensitive to the isospin asymmetry of the system. This is because the IMFs preferentially form in the forward and backward regions owing to the IMFs formation mechanism. In panels (e) and (f), we present $\sum N / \sum Z$ as a function of $E_{c.m.}/A$ in the non-transverse direction region, i.e., $\theta_{c.m.} < 70°$ and $\theta_{c.m.} > 110°$, and $\sum N / \sum Z$ in the non-transverse direction not only depend on the stiffness of

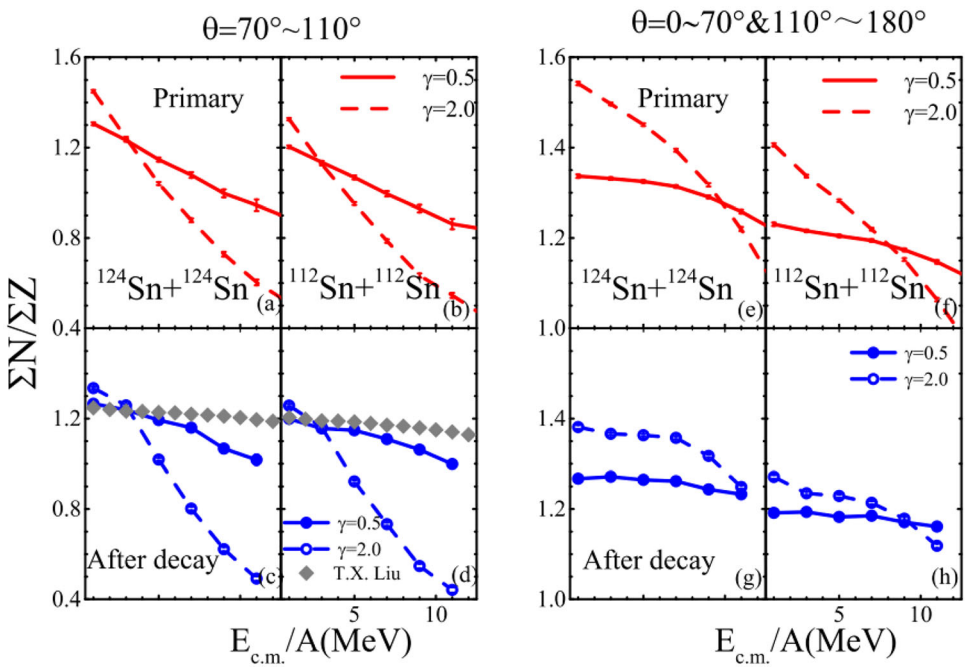


**Fig. 4** $\sum N/\sum Z$ as a function of the kinetic energy per nucleon for $^{124}$Sn+$^{124}$Sn (left four panels) and for $^{112}$Sn+$^{112}$Sn (right four panels). Panel **a**, **b**, **e** and **f** represent the results for the primary fragments, and **c**, **d**, **g** and **h** are the results for the cold fragments

the symmetry energy, but also on the isospin asymmetry of the systems.

The results of $\sum N/\sum Z$ of the IMFs after decay are plotted in panels (c) and (d) for the transverse direction and in panels (g) and (h) for the non-transverse direction. The secondary sequential decay mainly influences the $\sum N/\sum Z$ ratios in the lower kinetic energy region because the fragments with lower kinetic energy mainly consist of neutron-rich isotopes. However, the $\sum N/\sum Z$ ratios still maintain a sensitivity to the density dependence of the symmetry energy after sequential decay. In the transverse direction, the calculations indicate that the sensitivity of $\sum N/\sum Z$ increases as $E_{\mathrm{c.m.}}/A$ increases. We compared the calculated results in the transverse direction with the data (solid points in panels (c) and (d)) [50], which includes the $^{8}$Be contribution, to understand the model prediction. It is evident that the calculations with $\gamma$=0.5 are favored, and this conclusion is consistent with the constraints on $\gamma$ obtained with the *n*/*p* ratio, isospin diffusion, and isospin transport ratio as a function of rapidity [5, 54]. For $\sum N/\sum Z$ as a function of $E_{\mathrm{c.m.}}/A$ in the non-transverse direction, our calculations show that the values of $\sum N/\sum Z$ are not only sensitive to the symmetry energy, but also the isospin asymmetry of the systems. However, the sensitivity of $\sum N/\sum Z$ in the non-transverse direction is weaker compared to that in the transverse direction.

Finally, we analyze the double ratios of $\sum N/\sum Z$ for the two systems A $=^{124}$ Sn $+^{124}$ Sn and B $=^{112}$ Sn $+^{112}$ Sn, i.e.,

$$DR(N/Z) = \left(\sum N/\sum Z\right)_{\mathrm{A}} \Big/ \left(\sum N/\sum Z\right)_{\mathrm{B}}. \quad (9)$$

The idea of this double ratio is similar to the double neutron-to-proton ratio, which has been used to isolate the isospin effects and constrain the density dependence of the symmetry energy [6, 45, 54]. To obtain good statistics of the results of *DR*(*N*/*Z*) in the transverse direction, we performed simulations with 100,000 events. In Fig. 5a, we present the *DR*(*N*/*Z*) ratios for the cold fragments in the transverse direction for an experimental case such that $70^{\circ} \le \theta_{\mathrm{c.m.}} \le 110^{\circ}$. The shaded region with a solid pattern (dashed pattern) is the result obtained for $\gamma$=0.5 ($\gamma$=2.0). The *DR*(*N*/*Z*) ratios obtained for $\gamma = 2.0$ are larger than those obtained for the $\gamma = 0.5$ case. This can be observed from Fig. 3. These trends reflect the fact that the fragments originate from the composite system that survives the pre-equilibrium emission, as indicated in Ref. [6]. Compared to the data, the calculations for the case of $\gamma$=0.5 are favored. We also analyzed *DR*(*N*/*Z*) in the non-transverse direction, and the results are shown in panel (b). The calculations show that the sensitivity of *DR*(*N*/*Z*) to the stiffness of the symmetry energy is maintained in the non-transverse direction, and the *DR*(*N*/*Z*) in the non-transverse direction has good statistics because the IMFs are distributed in the forward and backward regions.

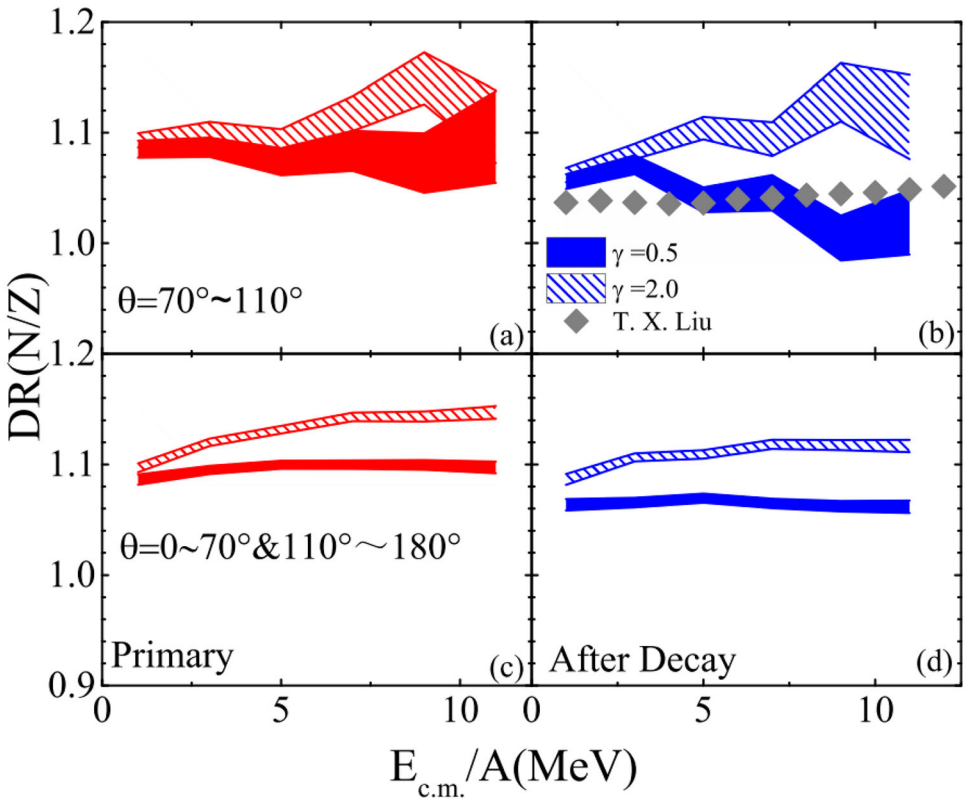


**Fig. 5** Double *N/Z* ratios as a function of the kinetic energy per nucleon. The top panels are the results for the transverse direction, and the bottom panels are the results for non-transverse direction

## 4 Summary and prospective

In summary, we investigated the isospin properties of intermediate mass fragments for the reaction $^{112,124}$Sn + $^{112,124}$Sn at a beam energy of 50 MeV per nucleon. Our results indicated that the average kinetic energy per nucleon of the fragments $\langle E_{\mathrm{c.m.}}/A \rangle$ as a function of $Z$ is sensitive to the density dependence of the symmetry energy, and this sensitivity does not change significantly by secondary sequential decay. Furthermore, the $\langle N \rangle / Z$ ratio of the IMFs as a function of the kinetic energy per nucleon is also sensitive to the density dependence of the symmetry energy. To circumvent the difficulties associated with cluster formation in transport model calculations, we also investigated the $\sum N / \sum Z$ and $DR(N/Z)$ ratios as a function of kinetic energy. The calculations revealed that both observables are sensitive to the density dependence of the symmetry energy, and the sensitivity was maintained even after secondary sequential decay. By comparing the calculations to the obtained data, the symmetry energy with $\gamma$=0.5 is favored. The results are consistent with the conclusions obtained by simultaneously describing the n/p ratios, isospin diffusion, and isospin transport ratio as a function of rapidity.

Nevertheless, the tight constraints on the symmetry energy still need more work. For example, the effects of the momentum-dependent symmetry potential should be well understood because the isospin-dependent momentum-dependent symmetry potential influences the cluster formation and the n/p ratio of the emitted nucleons [66, 67]. Thus, the curves of the average kinetic energy of the IMFs as a function of $Z$ are modified. The $\sum N / \sum Z$ ratios and $DR(N/Z)$ may also be influenced by the different signs associated with effective mass splitting. These points should be carefully investigated in the future. Our analysis and experimental studies [50] also suggest that a sequential decay model should be developed.

**Acknowledgements** Y. Zhang is thankful for the helpful discussions with Prof. M. B. Tsang.

**Author Contributions** All authors contributed to the study conception and design. Material preparation, data collection and analysis were performed by Li Li, Fang-Yuan Wang and Ying-Xun Zhang. The first draft of the manuscript was written by Ying-Xun Zhang and all authors commented on previous versions of the manuscript. All authors read and approved the final manuscript.

## References

1. B.-A. Li, L.-W. Chen, C.M. Ko, Recent progress and new challenges in isospin physics with heavy-ion reactions. Phys. Rep. **464**, 113 (2008). https://doi.org/10.1016/j.physrep.2008.04.005
2. M.B. Tsang, J.R. Stone, F. Camera et al., Constraints on the symmetry energy and neutron skins from experiments and theory.

Phys. Rev. C **86**, 015803 (2012). https://doi.org/10.1103/PhysRevC.86.015803
3. P. Danielewicz, Flow and the equation of state of nuclear matter. Nucl. Phys. A **685**, 368c (2001). https://doi.org/10.1016/S0375-9474(01)00554-1
4. L.-W. Chen, C.M. Ko, B.-A. Li, High-energy behavior of the nuclear symmetry potential in asymmetric nuclear matter. Phys. Rev. C **72**, 064606 (2005). https://doi.org/10.1103/PhysRevC.72.064606
5. M.B. Tsang, Y. Zhang, P. Danielewicz et al., Constraints on the density dependence of the symmetry energy. Phys. Rev. Lett. **102**, 122701 (2009). https://doi.org/10.1103/PhysRevLett.102.122701
6. M. Colonna, V. Banran, M. Di Toro et al., Isospin distillation with radial flow: A test of the nuclear symmetry energy. Phys. Rev. C **78**, 064618 (2008). https://doi.org/10.1103/PhysRevC.78.064618
7. Z.G. Xiao, R.J. Hu, H.Y. Wu et al., System dependence of the correlation function of IMFs in $^{36}$Ar $+^{112,124}$Sn at 35 MeV/u. Phys. Lett. B **639**, 436 (2006). https://doi.org/10.1016/j.physletb.2006.06.076
8. E.W. Cornell, T.M. Hamilton, D. Fox et al., Investigating the evolution of multifragmenting systems with fragment emission order. Phys. Rev. Lett. **77**, 4508 (1996). https://doi.org/10.1103/PhysRevLett.77.4508
9. E. Galichet, M.F. Rivet, B. Borderie et al., Isospin diffusion in $^{58}$Ni-induced reactions at intermediate energies. I. Experimental results. Phys. Rev. C **79**, 064614 (2009). https://doi.org/10.1103/PhysRevC.79.064614
10. T.X. Liu, W.G. Lynch, M.B. Tsang et al., Isospin diffusion observables in heavy-ion reactions. Phys. Rev. C **76**, 034603 (2007). https://doi.org/10.1103/PhysRevC.76.034603
11. Y. Zhang, J.L. Tian, W.J. Cheng et al., Long-time drift of the isospin degree of freedom in heavy ion collisions. Phys. Rev. C **95**, 041602(R) (2017). https://doi.org/10.1103/PhysRevC.95.041602
12. Y. Liu, Y.J. Wang, Y. Cui et al., Insights into the pion production mechanism and the symmetry energy at high density. Phys. Rev. C **103**, 014616 (2021). https://doi.org/10.1103/PhysRevC.103.014616
13. J. Estee, W.G. Lynch, C.Y. Tsang et al. (SπRIT Collaboration), Probing the symmetry energy with the spectral pion ratio. Phys. Rev. Lett. **126**, 162701 (2021). https://doi.org/10.1103/PhysRevLett.126.162701
14. Y. Zhang, M. Liu, C.-J. Xia et al., Constraints on the symmetry energy and its associated parameters from nuclei to neutron stars. Phys. Rev. C **101**, 034303 (2020). https://doi.org/10.1103/PhysRevC.101.034303
15. B. Li, N. Tang, F.-S. Zhang, Isospin effects of projectile fragmentation in a boltzmann-langevin approach. Chin. Phys. C 45, 084103 (2021). https://doi.org/10.1088/1674-1137/ac009a
16. J. Su, Constraining symmetry energy at subnormal density by isovector giant dipole resonances of spherical nuclei. Chin. Phys. C 43, 064109 (2019). https://doi.org/10.1088/1674-1137/43/6/064109
17. T.-G. Yue, L.-W. Chen, Z. Zhang, Y. Zhou, Constraints on the symmetry energy from PREX-II in the multimessenger era. arXiv:2102.05267
18. Z.-Q. Feng, Nuclear dynamics and particle production near threshold energies in heavy-ion collisions. Nucl. Sci. Tech. **29**(3), 40 (2018). https://doi.org/10.1007/s41365-018-0379-z
19. H. Yu, D.-Q. Fang, Y.-G. Ma, Investigation of the symmetry energy of nuclear matter using isospin-dependent quantum molecular dynamics. Nucl. Sci. Tech. **31**(6), 61 (2020). https://doi.org/10.1007/s41365-020-00766-x
20. J. Liu, C. Gao, N. Wan et al., Basic quantities of the equation of state in isospin asymmetric nuclear matter. Nucl. Sci. Tec. **32**(11), 117 (2021). https://doi.org/10.1007/s41365-021-00955-2
21. H. Zheng, S. Burrello, M. Colonna, V. Baran, Pre-equilibrium effects in charge-asymmetric low-energy reactions. Phys. Lett. B **769**, 424 (2017). https://doi.org/10.1016/j.physletb.2017.04.002
22. X. Jun, Constraining Isovector Nuclear Interactions with Giant Dipole Resonance and Neutron Skin in 208Pb from a Bayesian Approach. Chin. Phys. Lett. **38**, 04210 (2021). https://doi.org/10.1088/0256-307X/38/4/042101
23. B.P. Abbott et al., (LIGO scientific collaboration and virgo collaboration), GW170817: observation of gravitational waves from a binary neutron star inspiral. Phys. Rev. Lett. **119**, 161101 (2017). https://doi.org/10.1103/PhysRevLett.119.161101
24. B.P. Abbott et al., (LIGO scientific collaboration and virgo collaboration), GW170817: measurements of neutron star radii and equation of state. Phys. Rev. Lett. **121**, 161101 (2018). https://doi.org/10.1103/PhysRevLett.121.161101
25. E. Annala, T. Gorda, A. Kurkela et al., Gravitational-wave constraints on the neutron-star-matter equation of stategravitational-wave constraints on the neutron-star-matter equation of state phys. Rev. Rev. Lett. **120**, 172703 (2018). https://doi.org/10.1103/PhysRevLett.120.172703
26. F.J. Fattoyev, J. Piekarewicz, C.J. Horowitz, Neutron skins and neutron stars in the multimessenger era. Phys. Rev. Lett. **120**, 172702 (2018). https://doi.org/10.1103/PhysRevLett.120.172702
27. B.P. Abbott et al., (LIGO scientific collaboration and virgo collaboration), properties of the binary neutron star merger GW170817. Phys. Rev. X **9**, 011001 (2019). https://doi.org/10.1103/PhysRevX.9.011001
28. T. Malik, B.K. Agrawal, J.N. De et al., Tides in merging neutron stars: consistency of the GW170817 event with experimental data on finite nuclei. Phys. Rev. C **99**, 052801(R) (2019). https://doi.org/10.1103/PhysRevC.99.052801
29. N.B. Zhang, B.A. Li, Delineating effects of nuclear symmetry energy on the radii and tidal polarizabilities of neutron stars. J. Phys. G: Nucl. Part. Phys. **46**, 014002 (2019). https://doi.org/10.1088/1361-6471/aaef54
30. C.Y. Tsang, M.B. Tsang, P. Danielewicz et al., Insights on skyrme parameters from GW170817. Phys. Lett. B **796**, 1 (2019). https://doi.org/10.1016/j.physletb.2019.05.055
31. M.B. Tsang, W.G. Lynch, P. Danielewicz et al., Symmetry energy constraints from GW170817 and laboratory experiments. Phys. Lett. B **795**, 533 (2019). https://doi.org/10.1016/j.physletb.2019.06.059
32. C.-J. Jiang, Y. Qiang, D.-W. Guan et al., From finite nuclei to neutron stars: The essential role of high-order density dependence in effective forces. Chin. Phys. Lett. **38**, 052101 (2021). https://doi.org/10.1088/0256-307X/38/5/052101
33. J. Zhang, D. Wen, Y. Li, Constraint on nuclear symmetry energy imposed by f-mode oscillation of neutron stars. Commun. Theor. Phys. **73**, 115302 (2021). https://doi.org/10.1088/1572-9494/ac1669
34. B.-J. Cai, L.-W. Chen, Constraints on the skewness coefficient of symmetric nuclear matter within the nonlinear relativistic mean field model. Nucl. Sci. Tech. **28**, 185 (2017). https://doi.org/10.1007/s41365-017-0329-1
35. B.-A. Li, B.-J. Cai, L.-W. Chen et al., A theoretical overview of isospin and EOS effects in heavy-ion reactions at intermediate energies. arXiv:2201.09133
36. B.T. Reed, F.J. Fattoyev, C.J. Horowitz et al., Implications of PREX-2 on the equation of state of neutron-rich matter. Phys. Rev. Lett. **126**, 172503 (2021). https://doi.org/10.1103/PhysRevLett.126.172503
37. S.V. Pineda, K. Konig, D.M. Rossi et al., Charge radius of neutron-deficient $^{54}$Ni and symmetry energy constraints using the

difference in mirror pair charge radii. Phys. Rev. Lett. **127**, 182503 (2021). https://doi.org/10.1103/PhysRevLett.127.182503
38. R. Essick, I. Tews, P. Landry, A. Schwenk, Astrophysical constraints on the symmetry energy and the neutron skin of $^{208}$Pb with minimal modeling assumptions. Phys. Rev. Lett. **127**, 192701 (2021). https://doi.org/10.1103/PhysRevLett.127.192701
39. J. Xu, L.-W. Chen, M.Y.B. Tsang et al., Understanding transport simulations of heavy-ion collisions at 100A and 400A MeV: comparison of heavy-ion transport codes under controlled conditions. Phys. Rev. C **93**, 044609 (2016). https://doi.org/10.1103/PhysRevC.93.044609
40. Y. Zhang, Y. Wang, M. Colonna et al., Comparison of heavy-ion transport simulations: collision integral in a box. Phys. Rev. C **97**, 034625 (2018). https://doi.org/10.1103/PhysRevC.97.034625
41. A. Ono, J. Xu, M. Colonna et al., Comparison of heavy-ion transport simulations: collision integral with pions and Δ resonances in a box Phys. Rev. C **100**, 044617 (2019). https://doi.org/10.1103/PhysRevC.100.044617
42. M. Colonna, Y. Zhang, Y. Wang et al., Comparison of heavy-ion transport simulations: mean-field dynamics in a box. Phys. Rev. C **104**, 024603 (2021). https://doi.org/10.1103/PhysRevC.104.024603
43. H. Wolter, M. Colonna, D. Cozma, et al., submitted to Prog. Part. Nucl. Phys.
44. M.B. Tsang, W.A. Friedman, C.K. Gelbke et al., Isotopic scaling in nuclear reactions. Phys. Rev. Lett. **86**, 5023 (2001). https://doi.org/10.1103/PhysRevLett.86.5023
45. M.A. Famiano, T. Liu, W.G. Lynch et al., Neutron and proton transverse emission ratio measurements and the density dependence of the asymmetry term of the nuclear equation of state. Phys. Rev. Lett. **97**, 052701 (2006). https://doi.org/10.1103/PhysRevLett.97.052701
46. M.B. Tsang, T.X. Liu, L. Shi et al., Isospin diffusion and the nuclear symmetry energy in heavy ion reactions. Phys. Rev. Lett. **92**, 062701 (2004). https://doi.org/10.1103/PhysRevLett.92.062701
47. Y.-X. Zhang, C.-S. Zhou, J.-X. Chen, et. al., Correlation between the fragmentation modes and light charged particles emission in heavy ion collisions. Sci. China-Phys. Mech. Astron. **58**(11), 112002 (2015). https://doi.org/10.1007/s11433-015-5723-2
48. C.-W. Ma, Y.-G. Ma, Shannon information entropy in heavy-ion collisions. Prog. Part. Nucl. Phys. **99**, 120 (2018). https://doi.org/10.1016/j.ppnp.2018.01.002
49. C.-W. Ma, H.-L. Wei, X.-Q. Liu et al., Nuclear fragments in projectile fragmentation reactions. Prog. Part. Nucl. Phys. **121**, 10391 (2021). https://doi.org/10.1016/j.ppnp.2021.103911
50. T.X. Liu, W.G. Lynch, R.H. Showalter et al., Isospin observables from fragment energy spectra. Phys. Rev. C **86**, 024605 (2012). https://doi.org/10.1103/PhysRevC.86.024605
51. Y. Zhang, D.D.S. Coupland, P. Danielewicz et al., Influence of in-medium NN cross sections, symmetry potential, and impact parameter on isospin observables. Phys. Rev. C **85**, 024602 (2012). https://doi.org/10.1103/PhysRevC.85.024602
52. Y. Zhang, Z. Li, Probing the density dependence of the symmetry potential with peripheral heavy-ion collisions. Phys. Rev. C **71**, 024604 (2005). https://doi.org/10.1103/PhysRevC.71.024604
53. Y. Zhang, Z. Li, Elliptic flow and system size dependence of transition energies at intermediate energies. Phys. Rev. C **74**, 014602 (2006). https://doi.org/10.1103/PhysRevC.74.014602
54. Y. Zhang, P. Danielewicz, M. Famiano et al., The influence of cluster emission and the symmetry energy on neutron-proton spectral double ratios. Phys. Lett. B **664**, 145 (2008). https://doi.org/10.1016/j.physletb.2008.03.075
55. Y.-X. Zhang, N. Wang, Q.-F. Li et al., Progress of quantum molecular dynamics model and its applications in heavy ion collisions. Front. Phys. **15**(5), 54301 (2020). https://doi.org/10.1007/s11467-020-0961-9
56. R.J. Charity, M.A. McMahan, G.J. Wozniak et al., Systematics of complex fragment emission in niobium-induced reactions. Nucl. Phys. A **483**, 371 (1988). https://doi.org/10.1016/0375-9474(88)90542-8
57. R. J. Charity, in Joint ICTP-AIEA Advanced Workshop on Model Codes for Spallation Reactions (IAEA, Vienna, 2008), Report INDC(NDC)-0530
58. S. Jun, L. Zhu, C.-Y. Huang, W.-J. Xie et al., Correlation between symmetry energy and effective k-mass splitting with an improved isospin- and momentum-dependent interaction. Phys. Rev. C **94**, 034619 (2016). https://doi.org/10.1103/PhysRevC.94.034619
59. W.-J. Xie, S. Jun, L. Zhu et al., Neutron-proton effective mass splitting in a boltzmann-langevin approach. Phys. Rev. C **88**, 061601(R) (2013). https://doi.org/10.1103/PhysRevC.88.061601
60. H.H. Gutbrod, A. Sandoval, P.J. Johansen et al., Final-state interactions in the production of hydrogen and helium isotopes by relativistic heavy ions on uranium. Phys. Rev. Lett. **37**, 667 (1976). https://doi.org/10.1103/PhysRevLett.37.667
61. E. Renshaw, S.J. Yennello, K. Kwiatkowski et al., Analyzing powers and isotope ratios for the $^{nat}$Ag(p→ intermediate-mass fragment) reaction at 200 MeV Phys. Rev. C **44**, 2618 (1991). https://doi.org/10.1103/PhysRevC.44.2618
62. W. Neubert, A.S. Botvina, What is the physics behind the $^{3}He$-$^{4}He$ anomaly? Eur. Phys. J. A **7**, 101 (2000). https://doi.org/10.1007/s100500050016
63. L. Li, Y. Zhang, Z. Li et al., Impact parameter smearing effects on isospin sensitive observables in heavy ion collisions. Phys. Rev. C **97**, 044606 (2018). https://doi.org/10.1103/PhysRevC.97.044606
64. E. Plagnol, J. Łukasik, G. Auger et al., Onset of midvelocity emissions in symmetric heavy ion reactions. Phys. Rev. C **61**, 014606 (1999). https://doi.org/10.1103/PhysRevC.61.014606
65. L. Phair, D.R. Bowman, C.K. Gelbke et al., Impact-parameter filters for $^{36}$Ar+$^{197}$Au collisions at E/A = 50, 80 and 110 MeV. Nucl. Phys. A **548**, 489 (1992). https://doi.org/10.1016/0375-9474(92)90697-I
66. D.D.S. Coupland, W.G. Lynch, M.B. Tsang et al., Influence of transport variables on isospin transport ratios. Phys. Rev. C **84**, 054603 (2011). https://doi.org/10.1103/PhysRevC.84.054603
67. Y. Zhang, M.B. Tsang, Z. Lia et al., Constraints on nucleon effective mass splitting with heavy ion collisions. Phys. Lett. B **732**, 186–190 (2014). https://doi.org/10.1016/j.physletb.2014.03.030